THE JOURNAL OF PHYSICAL CHEMISTRY C
A JOURNAL OF THE AMERICAN CHEMICAL SOCIETY

pubs.acs.org/JPCC

Article

On the Formation of Honeycomb Superlattices from PbSe Quantum Dots: The Role of Solvent-Mediated Repulsion and Facet-to-Facet Attraction in NC Self-Assembly and Alignment

Maaike M. van der Sluijs, Dinja Sanders, Kevin J. Jansen, Giuseppe Soligno, Daniel Vanmaekelbergh, and Joep L. Peters*

Cite This: J. Phys. Chem. C 2022, 126, 986−996

Read Online

ACCESS | Metrics & More | Article Recommendations | Supporting Information

ABSTRACT: Semiconductor superstructures made from assembled and epitaxially connected colloidal nanocrystals (NCs) hold promise for crystalline solids with atomic and nanoscale periodicity, whereby the band structure can be tuned by the geometry. The formation of especially the honeycomb superstructure on a liquid substrate is far from understood and suffers from weak replicability. Here, we introduce 1,4-butanediol as an unreactive substrate component, which is mixed with reactive ethylene glycol to tune for optimal reactivity. It shows us that the honeycomb superlattice has a NC precursor state before oriented attachment occurs, in the form of a self-assembled hexagonal bilayer. We propose that the difference between the formation of the square or honeycomb superstructure occurs during the self-assembly phase. To form a honeycomb superstructure, it is crucial to stabilize the hexagonal bilayer in the presence of solvent-mediated repulsion. In contrast, a square superstructure benefits from the contraction of a hexagonal monolayer due to the absence of a solvent. A second experiment shows the very last stage of the process, where the increasing alignment of NCs is quantified using selected-area electron diffraction (SAED). The combination of transmission electron microscopy (TEM), SAED, and tomography used in these experiments shows that the (100)/(100) facet-to-facet attraction is the main driving force for NC alignment and attachment. These findings are validated by coarse-grained molecular dynamic simulations, where we show that an optimal NC repulsion is crucial to create the honeycomb superstructure.

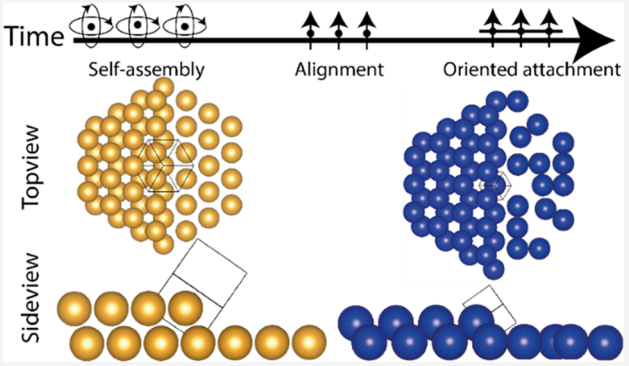

INTRODUCTION

For the fabrication of inorganic crystals that feature atomic and nanoscale periodicity, top-down lithographic approaches have been used.[1] However, due to high costs and wavelength limitations, this method reaches its limits at a period of roughly 20 nm.[2] A cheaper method, while achieving even smaller features (down to 6.5 nm), would be the well-controlled oriented attachment of monodisperse nanocrystals.[3] In the classical crystal growth model, monomers are attached one-by-one to the growing crystal. By utilizing differences in chemical composition and reactivity of facets, it is often possible to manipulate the direction of this growth. In oriented attachment, this principle of distinctive facet reactivity also holds but now for the facet-specific attachment of nanocrystals to form a periodic solid. Such superstructures have been obtained with a variety of nanocrystals and under different conditions. Advanced structures and control of the process have only been obtained in apolar solvents by attachment via stoichiometric facets.[4−8]

Lead chalcogenide NCs covered by deprotonated fatty acids lead this research field.[3,5,6] These NCs have six chemically identical stoichiometric {100} crystal facets and eight non-stoichiometric {111} facets. It has been shown that the {100} facets can epitaxially attach to a (100) facet of a neighboring NC, if ligands are removed. Attachment does not happen for the inactive {111} facets, where ligands are bound much stronger and therefore not easily removed.[9] The epitaxial connection ensures strong electronic coupling between NCs[10,11] and may even result in a specific electronic band structure depending on the geometry of the superstructure.[12−14] Of special interest is the two-dimensional (2D) silicene-type honeycomb superstructure, which could combine typical semiconductor properties, with Dirac cones in the valence and conduction band.[13,14] Unfortunately, a full

Received: August 21, 2021
Revised: December 17, 2021
Published: January 5, 2022

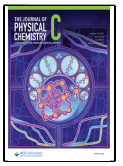

https://doi.org/10.1021/acs.jpcc.1c07430
J. Phys. Chem. C 2022, 126, 986−996

understanding and control of the honeycomb superstructure formation from PbSe NCs has not yet been achieved.

A growing number of studies demonstrate the importance of the NC organization preceding oriented attachment.[15−18] A study by Geuchies et al. (using grazing-incidence small- and wide-angle X-ray scattering, GISAXS/GIWAXS) showed that a hexagonal assembly of PbSe NCs contracted in-plane and transformed gradually to a square assembly, prior to NC attachment with (100)/(100) interactions as the driving force.[19] This structural contraction from the hexagonal NC assembly to a square assembly is necessary to reach the correct bonding geometry and to bring the opposing (100)/(100) facets close enough. This transition is presumably due to the soft character of the ligand shell and the removal of residual solvent.[20−23] After that, the ligands strip from the surface, NCs align, and stoichiometric {100} facets become free, which makes a reduction of the surface energy possible by an epitaxial connection (attachment) between opposing {100} facets.[24−26] To form structures with other nanogeometries, i.e., honeycomb structures, the continued presence of the residual solvent in the ligand shell or additional unbound ligands was found to be essential.[23,27,28]

In this work, we use transmission electron microscopy (TEM), selected-area electron diffraction (SAED) and molecular dynamic simulations to study the honeycomb superstructure formation by casting a PbSe NC dispersion on ethylene glycol and controlling solvent evaporation. Samples, taken during the process, were immediately placed under vacuum to preserve the sampled superstructure, enabling an ex situ, real-time study of self-assembly and attachment. The first experiment utilizes 1,4-butanediol, mixed in varying ratios with the ethylene glycol liquid substrate, to slow down the ligand stripping and therefore the attachment of NCs. It provides a powerful method to balance and study the attraction between the {100} facets. NCs which are too reactive attach quickly and form uncontrolled structures. In contrast, without ligand stripping, NCs do not align and stay in the precursor state of hexagonal mono- or bilayers. The second experiment studies the last stage; NCs are then organized in a hexagonal bilayer and are initially only slightly oriented with a preferred orientation of the ⟨111⟩ axis upwards. Over time, NC−NC alignment becomes more and more pronounced, until attachment occurs. To complement the experiments, we use coarse-grained molecular dynamic simulations. With these modeling results, we substantiate the hypothesis that solvent inclusion in the NC ligand shell allows the formation of the hexagonal bilayer precursor phase and provides the stability and NC density necessary to form honeycomb superstructures. Without these space-filling molecules, the NC precursor phase is not stable enough, resulting in disordered or square structures.

METHODS

Chemicals. Benzene (99.8%, anhydrous), *n*-butanol (99.8%, anhydrous), 1-chloropentane (99%), cyclohexyl isocyanide (98%), diphenylphosphine (98%), hexane (mixture of isomers, ≥99%, anhydrous), isopropanol (99.5%, anhydrous), lead acetate trihydrate (≥99.99%), methanol (99.8%, anhydrous), 1-octadecene (90%), octane (≥99%, anhydrous), oleic acid (90%), pyrrolidine (≥99%), selenium powder (99.99%, −100 mesh), tetrachloroethylene (≥99%, anhydrous), toluene (99.8%, anhydrous), triethylamine (≥99%), trifluoroacetic acid (99%), trifluoroacetic anhydride (≥99%), trimethylbenzene (98%), and trioctylphosphine (90%) were purchased from Sigma-Aldrich and used without further purification. Lead (II) oxide (99.999+%) was purchased from Strem Chemicals. 1,4-Butanediol (BD, 99%, ReagentPlus), diethylene glycol (DEG, 99%), diphenyl ether (≥99%), ethylene glycol (EG, 99.8%, anhydrous), and hexadecane (≥99%) were purchased from Sigma-Aldrich and degassed under vacuum for ∼14 h at 60 °C prior use. For superlattice formation, a distillation of the EG did not result in a significant difference in the quality of the formed superlattice (see Figure S1).

PbSe Synthesis. PbSe NCs were synthesized with two different procedures. The first method was developed by Steckel et al.[29] In brief, 4.77 g of $Pb(C_2H_3O_2)_2{\cdot}3H_2O$, 10.35 g of oleic acid (Pb/oleic acid ratio of 1:2.91), and 39.75 g of 1-octadecene were mixed and degassed at 120 °C under vacuum for 5 h to remove water and acetate. The selenium precursor was prepared by dissolving 3.52 g of selenium powder in 0.41 g of diphenylphosphine and 46.59 g of trioctylphosphine. The selenium precursor was injected into a heated solution of the lead precursor (180 °C) under vigorous stirring. After 70 s, the reaction was quenched via injection of 30 mL of a methanol/butanol mixture (1:2). The mixture was centrifuged, and the black residue was dispersed in toluene (10 mL). Methanol was added (8 mL) to precipitate the suspension, which was subsequently centrifuged. The black residue was dispersed in toluene, and the cycle was repeated two more times. The second method was developed by Campos et al.,[30] with a lead oleate precursor ($Pb(oleate)_2$) prepared via the method of Hendricks et al.[31] In short, lead(II) oxide (10.00 g, 44.8 mmol) and acetonitrile (∼20 mL) were added to a 100 mL round-bottom flask. The suspension was stirred while being cooled in an ice bath, after which trifluoroacetic acid (0.7 mL, 8.96 mmol, 0.2 equiv) and trifluoroacetic anhydride (6.2 mL, 44.8 mmol, 1 equiv) were added. After 10 min, the yellow lead oxide dissolved, resulting in a clear and colorless solution that was allowed to warm to room temperature. Oleic acid (25.44 g, 90.05 mmol, 2.01 equiv), isopropanol (∼180 mL), and triethylamine (10.25 g, 101.25 mmol, 2.26 equiv) were added into a 500 mL Erlenmeyer flask. The lead trifluoroacetate solution was slowly added to the oleic acid solution while stirring, resulting in the formation of a white precipitate. The mixture was heated to reflux, to dissolve the precipitate, after which a clear and colorless solution was obtained. The heat was turned off, and the flask was allowed to cool slowly to room temperature, followed by further cooling in a −20 °C freezer for >2 h. The resulting white powder was isolated by suction filtration using a glass fritted funnel, and the filtrate was thoroughly washed with methanol (3 × 300 mL). Large pieces were crushed to get a white powder, which was subsequently dried under vacuum for >6 h to get a fluffy white $Pb(oleate)_2$ powder. Which was reacted with the selenium precursor discussed below.

Selenium Precursor. The selenium precursor (*N*-cyclohexylpyrrolidine-1-carboselenoamide) was prepared by mixing selenium (0.71 g, 9.0 mmol), pyrrolidine (0.64 g, 9.0 mmol), cyclohexyl isocyanide (0.983 g, 9.0 mmol), and 10 mL of toluene. This mixture was heated to ∼100 °C until the solution turned clear. Additional pyrrolidine and/or cyclohexyl isocyanide was added if not all selenium reacted. The mixture was allowed to cool to room temperature where the selenourea precipitated. The liquid was decanted, and the obtained white solid was placed under vacuum for 24 h. Subsequently, the

https://doi.org/10.1021/acs.jpcc.1c07430
J. Phys. Chem. C 2022, 126, 986−996

solid was redissolved in 10 mL of toluene at 100 °C and allowed to cool down. The precipitate was filtered and the solid was placed under vacuum for another 24 h. The synthesis of PbSe NCs was performed in a Schlenk line, where 1.6 g (2.08 mmol, 1.2 equiv) of $Pb(oleate)_2$ was dissolved in 140 mL of hexadecane in a 250 mL three-neck flask. Then, 0.45 g (1.7 mmol, 1 equiv) of *N*-cyclohexylpyrrolidine-1-carboselenoamide was dissolved in 8 mL of diphenyl ether. Both precursors were heated to 100 °C to yield clear colorless solutions. The selenourea was quickly injected into the $Pb(oleate)_2$ solution, which turned brown in approximately 8 s. After 110 min, the reaction was cooled down with an ice bath and brought inside the glovebox. Then, 90 mL of *n*-butanol and 60 mL of methanol were added to precipitate NCs. The mixture was centrifuged, and the black residue was dispersed in 10 mL of toluene. This solution was washed three more times with methanol. The ligand density was determined via a previously published method.[9] We used NMR spectroscopy to determine if no free ligands were present and FTIR with a $Pb(oleate)_2$ calibration curve to determine the number of ligands per NC (see Supporting Information 2).

Superstructure Formation. All experiments were performed based on the experimental procedure as previously reported.[32] A small Petri dish (Ø 27 mm) was filled with 6.5 mL of ethylene glycol (or a mixture of EG and BD), creating a flat surface. This Petri dish was placed in a bigger Petri dish containing 2 mL of toluene. Subsequently, 350 μL of a diluted NC solution (7.7×10^{-8} M) in toluene was dropcasted on top of the 6.5 mL of EG (or a mixture), resulting in the height of ~0.061 cm, and both Petri dishes were covered with a beaker (400 mL). The honeycomb structure was formed on top of the liquid substrate during 15 h of slow toluene evaporation and could then be transferred to any substrate. The whole experiment is performed in a glovebox containing <0.1 ppm O_2, free of amines and other volatile gasses. The superstructure formation was successful for NCs with sizes between 5 and 7 nm. To minimize distortion, every sample in the time series (Figure 3) was prepared independently.

FTIR measurements were performed with a Bruker Vertex 70. A special airtight liquid cell was used, purchased from International Crystal Laboratories, with a path length of 0.5 mm and two KBr crystals at the back and front side to make it transparent for IR light. Spectra were recorded from 400 to 7500 cm^{-1}, with a KBr beam splitter, a DLaTGS D301 detector, and a mid IR source. For all of the measurements, tetrachloroethylene was used as a solvent. A calibration curve with $Pb(oleate)_2$ was used to determine the concentration ligands on NCs. The NC concentration was determined by the integration of the exciton peak.[33]

^{1}H NMR measurements were performed using an Agilent MRF400 equipped with a OneNMR probe and Optima Tune system. Spectra were recorded according to the following parameters: 400 MHz, $CDCl_3$ 25 °C. PbSe NCs were measured to determine if there were free ligands or other pollution present. Measurements of PbSe were performed using a longer relaxation delay (30 s) to allow complete relaxation. For NC-$Pb(oleate)_2$ Δ = 5.54 (m, 4H, HC = CH), 2.37 (t, 4H, 3JHH = 7.3 Hz, CH_2), 2.15 (m, 8H, CH_2), 1.77 (p, 4H, 3JHH = 7.8 Hz, CH_2), 1.5−1.2 (m, 42H, CH_2), and 0.93 (t, 6H, 3JHH = 6.7 Hz, CH_3).

TEM and SAED measurements were performed at a Philips Tecnai operating at 200 kV. In bright-field TEM, the contrast in the images scales relative to the highest contrast in the image; therefore, without additional measures quantitative comparison between different samples is not possible. To ensure the reproducibility of the measurement of the SAED peak width, the sample needs to be perpendicular to the electron beam while it is made sure that the diffraction peaks do not oversaturate the detector (see example in the main text and Supporting Information 5).

RESULTS AND DISCUSSION

In Situ Sampling of Nanocrystal Structures, Avoiding Perturbative Drying Effects. The typical synthesis for two-dimensional PbSe honeycomb superstructures is as follows: a PbSe quantum dot dispersion is dropcasted on an ethylene glycol (EG) liquid substrate, after which the toluene solvent evaporates under atmospheric nitrogen pressure[3] or under nearly solvent-saturated conditions.[32] After toluene evaporation, NCs were shown to float on top of the EG.[34] The EG plays a crucial role in the experiment, as it gradually removes ligands from the NC surface and makes {100} NC facets available for attachment.[3,6,9] The mechanism behind oleate removal by EG is not yet fully understood; however, in literature, two mechanisms have been suggested. When oleate ligands are considered to be X-type,[33,35,36] a proton transfer could induce displacement and exchange of the oleate ligand.[37] Previously, short-chain alcohols were suggested to enable this proton transfer to ligands.[35] More recent work has shown that amines injected in the EG liquid can induce epitaxial fusion in assembled PbSe NCs.[25,38] The amines (or other L-type ligands) induce ligand displacement as a metal carboxylate complex (Z-type displacement of lead oleate) from the NC surface, allowing attachment between bare {100} facets.[39] Although these publications have given tentative hints at a mechanism for ligand removal during superstructure formation, a complete understanding has not yet been achieved (see Supporting Information 1).[38] As soon as enough ligands have been stripped or exchanged, the facets become reactive and attachment can occur. Often, this results in a superstructure which is a mixture of different geometries instead of an ordered superstructure. We hypothesized that slowing the removal of ligands with an effectively less reactive liquid substrate would give us a method to improve control over the superstructure formation, even when using highly reactive NCs with a low ligand density. We narrowed the search by concentrating on a compound with similar properties as EG; it should be a liquid with two hydroxide groups to keep it barely mixable with apolar NCs solvents.

In Figure 1, TEM images show the results of casting the dispersion on 100% 1,4-butanediol (BD), which has two hydroxide groups and the proper melting point. As can be observed in the upper left of Figure 1a and the upper left of Figure 1b, monolayers are (pseudo-)hexagonally ordered, and NCs show no attachment, indicating that {100} facets have a significantly lower reactivity. We concluded that BD is not able to remove ligands from PbSe NCs on similar time scales as EG, making it a good candidate to vary the liquid substrate reactivity. Nevertheless, as shown in Figure S1, at higher temperatures, BD can induce removal of sufficient ligands to induce attachment.

It is important to note distinct differences in the double layers of these samples. In Figure 1a, the hexagonal bilayer is preserved with random orientation of NCs, as seen in the SAED inset, which shows full diffraction rings. The double layer in Figure 1b shows a structural change with a preferred

https://doi.org/10.1021/acs.jpcc.1c07430
J. Phys. Chem. C 2022, 126, 986−996

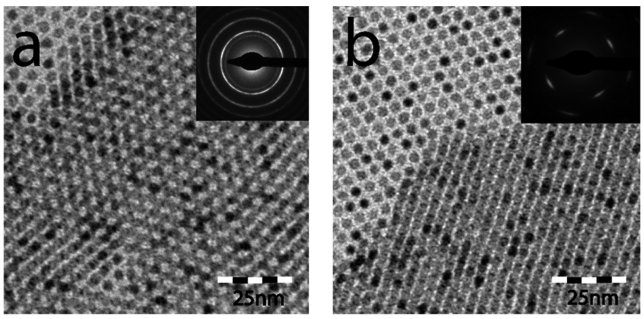

Figure 1. Two examples of self-assembled mono- and bilayer PbSe NCs formed over a 15 h experiment on 100% BD, in which we waited (a) 5 s and (b) 10 min between sampling and applying vacuum to "freeze" the sample. The small amount of toluene remaining on the sample does not result in strong turbulence during evaporation. However, when waiting before vacuum application, the organization of NCs changed from a hexagonal mono- or bilayer with random orientation (a) to a denser quasihexagonal mono- or bilayer with a preferred orientation of NCs with a (100) facet upwards (b).

orientation of NCs. This difference is attributed to the TEM sample treatment immediately after sampling of the superstructure. Prompt placement of the TEM sample under vacuum, in the small antechamber of the glovebox, "freezes" the structure and retains randomly rotated NCs (Figure 1a). Thus, the NC system that is absorbed at the interface or NCs which are present in a thin layer of toluene can be collected and preserved. Waiting too long before applying the vacuum allows evaporation of the residual solvent present in the ligand shell. Then, the NC shape becomes a more prominent factor, which induces structural changes in the superstructure and the preferred orientation of NCs. In three-dimensional structures (3D), a similar effect is observed in several NC systems, where it is described as the Bain deformation.[23,27,28,40−46] In all experiments presented below, the TEM samples were placed under vacuum immediately after sampling, "freezing" the superstructures as they have formed on the liquid substrate. The next step is to synthesize PbSe superstructures on the mixtures of BD and EG, to tune the superstructure attachment.

Tuning the NC Reactivity, Utilizing the Liquid Substrate. The conditions for these experiments are similar to previously described; slow solvent evaporation occurs under a nearly saturated toluene gas phase above the glycol/NC dispersion system (see Figure S5).[32] For this experiment, we used 7 nm PbSe NCs with a relatively low ligand density of 2.2 oleate/nm^2, as determined by FTIR and NMR (see Supporting Information 2). In Figure 2, we increased the ratio of BD to EG going from a 0:1 (a) to a 3.33:1 ratio (f). Without the addition of BD, attachment of NCs is observed, resulting in disordered nonperiodic structures (Figure 2a). With an increasing ratio of BD:EG, the degree of nanoscale periodicity increases, forming larger periodic superstructures with a honeycomb geometry (Figure 2b−d). The optimal liquid substrate mixture has a BD:EG ratio of 1:1.17, yielding long-range honeycomb superstructures with areas up to 10 μm^2 (Figure 2d). This long-range order is also illustrated by Fourier transforms (Figure S6). At the same time, the SAED image inset shows six sharp peaks on the 220 ring, indicative of NCs oriented with their ⟨111⟩ axis perpendicular to the substrate and no rotational freedom within the plane. With this orientation, three of the {100} facets face the {100} facets of neighboring NCs, forming a honeycomb structure.[6] A further increase of the BD:EG ratio results in unattached NCs ordered in mixed phases of hexagonal mono- and bilayers (Figure 2e, 2f). It is important to note that while these hexagonal bilayers look exactly like attached honeycomb superstructures in TEM images (see Supporting Information 3, Figure S7 for a detailed

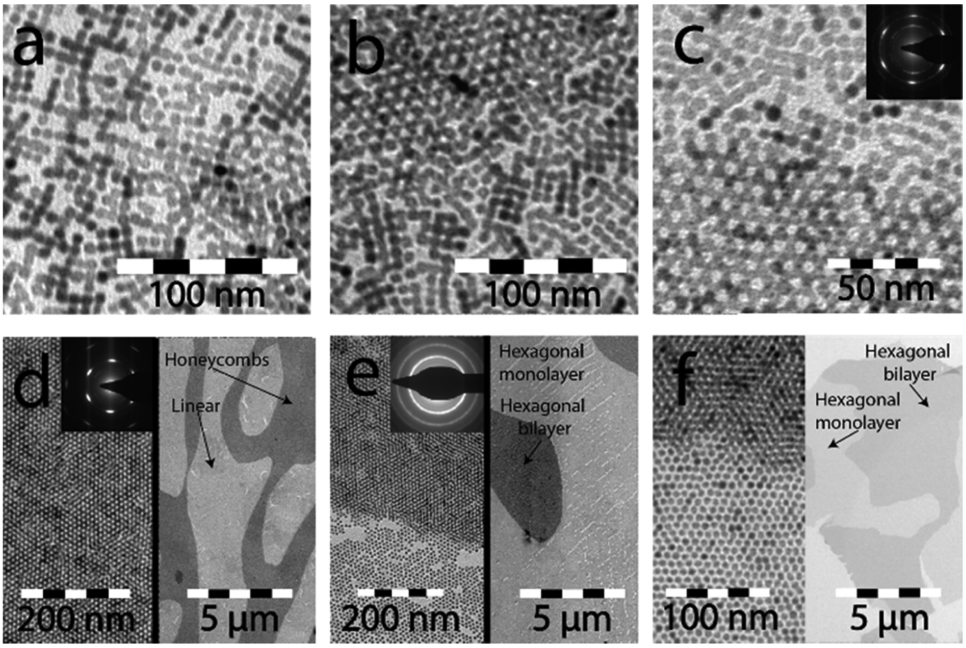

Figure 2. Honeycomb formation with an increasing concentration of 1,4-butanediol. The amount of 1,4-butanediol to ethylene glycol is, respectively, in (a) 0:6.5, (b) 1:5.5, (c) 2:4.5, (d) 3:3.5, (e) 4:2.5, and (f) 5:1.5 mL. The quantity and quality of the honeycomb structure improve with an increasing amount of BD, until no attachment is observed in (e) and (f). The insets in (d) and (e) are the SAED patterns of the bilayer area, showing strongly aligned and attached NCs in (d) and NCs with random orientations in (e). The right part of (d−f) shows a lower magnification TEM image, where the large domains of a linearly attached (see Figure S10a), honeycomb and self-assembled structures are visible.

https://doi.org/10.1021/acs.jpcc.1c07430
J. Phys. Chem. C 2022, 126, 986−996

comparison), the SAED image inset still shows rings, i.e., random orientation, confirming that NCs are not attached.

These results demonstrate the tremendous improvement in quantity and quality of the honeycomb structure with an increase in the relative amount of BD in the liquid substrate. The addition of the less reactive BD to EG provides a direct method to tune the formation of superstructures for NCs with different ligand densities. The results presented in Figure 2 confirm that ligand removal from the NC surface by EG is crucial to induce attachment of {100} facets, which is driven by surface energy reduction. They also suggest that the hexagonal bilayer is a precursor phase to the honeycomb superstructure, something additionally inferred from the similarities of the nanoscale and microscale organization of NCs between Figure 2d, 2e and 2f.

Final Stage of Alignment and Attachment, Facet-to-Facet Interactions. Below, we show a second experiment that monitors the formation of PbSe NC honeycomb superlattices in real time, confirming the key role of (100)/(100) facet-to-facet interactions in aligning NCs. Ideally, this study involves GISAXS/GIWAXS, as utilized in previous studies.[19,38,40,47] However, the formation of honeycomb structures requires ultraslow evaporation of the toluene solvent over 15 h in a nearly closed system under an inert atmosphere. In principle, in situ X-ray measurements over such a long period are possible. Nevertheless, they demand long occupation of the synchrotron measurement station, while self-assembling structures might be prone to beam damage and residual oxidation, making in situ GISAXS/GIWAXS very demanding. We have chosen for an ex situ, real-time study of superlattice formation by monitoring the sample at gradually longer times of toluene evaporation using TEM, tomography, and SAED. To avoid ex situ drying effects and preserve the in situ state of the structure (see above), the samples were immediately placed under vacuum. Figure 3 shows the representative TEM images of samples obtained after 3, 9, and 15 h of slow toluene evaporation at 20 °C for 6.1 nm PbSe NCs with a medium ligand density of 3.7 oleate/nm^2, as determined by FTIR and NMR (see Supporting Information 2, additional results are presented in Figures S8 and S9). We dropcasted the equivalent of approximately 1.5 monolayers of PbSe NCs on the liquid substrate surface. After 1−3 h (Figure 3a left, S8), only some of the NCs are present at the interface, while the rest is still suspended. The SAED diffractogram inset shows two rings corresponding to 200 and 220 diffraction rings with uniform intensity, an indication that NCs near an interface still have a random orientation.

The samples acquired at 6−12 h (Figure 3a middle and S8) show an increased density of NCs resulting in mono- and bilayers with a hexagonal geometry. The number of NCs on the TEM grid suggests that all NCs originally present in the dispersion are now at, or close to the interface. The SAED diffractogram inset top right shows that NCs in the monolayer are not aligned and thus still have random orientations. This is in line with GISAXS/GIWAXS patterns obtained previously for experiments with more rapid toluene evaporation.[19] However, bilayers show SAED patterns (top left), with a lower intensity on the 200 ring, a relatively strong intensity on the 220 ring, and the occurrence of six broad spots. These spots originate from an interference pattern of diffraction on the three sets of {110} crystal planes, showing that the ⟨111⟩ axis of NCs is oriented vertically to the interface, while NCs have limited rotational freedom. Thus, these bilayers should

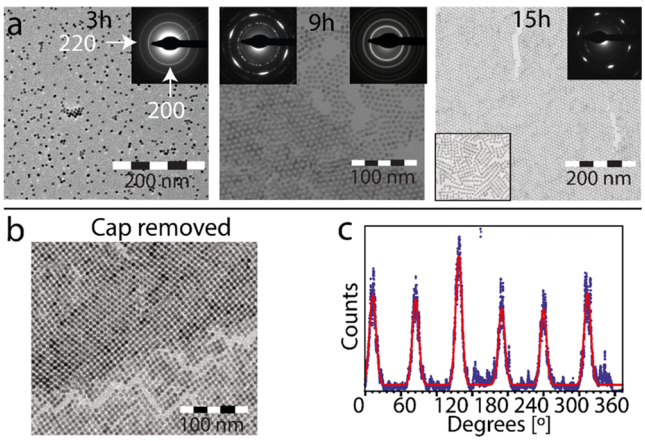

Figure 3. Real-time, ex situ study of the formation of a honeycomb superlattice. (a) TEM images of samples obtained by horizontal contact of TEM grids with the toluene−air interface, after 3, 9, and 15 h of experiment time. The sample at 9 h shows PbSe NC hexagonal mono- and bilayers. The upper-left inset shows the SAED of a bilayer: the spots indicate limited random orientation. The upper-right inset is a diffractogram of the hexagonal monolayer, indicating random NC orientations. After 15 h, all NCs in the bilayer are oriented with the ⟨111⟩ axis perpendicular to the plane of the superlattice. The lower-left TEM inset of the hexagonal monolayer at 15 h shows that linear structures have been formed as well. (b) TEM image of the superstructure formed after 3 h of experiment time and an additional 1 h after the removal of the cap (resulting in a low solvent vapor pressure). (c) Width of the six spots on the 220 ring after 9 h and the background scattering intensity on the azimuthal trace are analyzed using Gaussian fits (red). The values are presented in Table 1 and discussed in the text.

not be considered as consisting of "hard" spheres with a random orientation; the gradual alignment is due to NC rotations that try to maximize the attractions between the {100} facets of NC neighbors in the hexagonal bilayer.

The samples acquired after 15, and even 24 h (Figures 3a right, S8, and S9), show large bilayer domains. The SAED inset now shows almost no intensity on the 200 ring, while the 220 ring has six intense and small-angled spots, indicative of improved ⟨111⟩ orientation and alignment in the bilayer superstructure. This means that {100} facets must have a 45° orientation with respect to the plane, and it is very hard to discern from these TEM pictures whether attachment has already taken place (see below).

Besides large bilayer domains, monolayer domains are observed as well. In the monolayer (Figure 3a right, left corner inset), NCs are clearly attached in a linear geometry and oriented with {100} facets upwards (Figure S10a). These linear structures imply a symmetry breaking, as bonding sites are available in two orthogonal directions; the origin of this symmetry breaking is not well understood. The SAED and a Fourier transform of linear structures in Figure S10 show that although NCs are linearly attached, they are still organized in a disordered hexagonal symmetry. This indicates that unattached NCs in the hexagonal monolayer attach via opposing (100) facets that are vertically oriented in these linear structures while retaining some of their original position. Attachment of NCs in this area is an indication that NCs in the bilayer are attached as well.

Formation of Square versus Honeycomb Superstructures, the Importance of Solvent Inclusion. As was previously shown in Figure 1, the presence of residual

https://doi.org/10.1021/acs.jpcc.1c07430
J. Phys. Chem. C 2022, 126, 986−996

solvent in the ligand corona already plays a huge role in the geometry observed in the sample. A similar phenomenon was observed during the formation of the superstructures in Figure 3. When the cap of the setup is removed at different times during the experiment, the solvent vapor pressure drops and if superstructure formation is allowed to continue for another hour, different structures than those under near solvent saturation are formed. If the cap is removed during the first 3 h, only some of the NCs are present at the interface while the rest is still suspended (Figure 3a left). As shown in Figure 3b, an experiment continued at low solvent pressure for 1 h forms a superstructure with a square geometry, for which the detailed formation mechanism has been described before.[19] However, if the cap was removed in a much later stage of the process, after 6−12 h, the self-assembled hexagonal double layer evolved into an attached honeycomb structure. *It suggests that the difference in the formation of square or honeycomb structures occurs during self-assembly, prior to NC alignment and attachment*. The solvent makes up approximately 40% of the space in a self-assembled hexagonal layer, compared to ∼20 and ∼40% for the NC core and ligands, respectively, as shown by a simple calculation in Supporting Information 4. It is therefore no surprise that the NC organization in a self-assembled superlattice can change by solvent removal. This effect was previously described in literature for several NC systems.[22,27,40,48−50]

For the honeycomb formation, it is beneficial to have an ordered, unattached, "hard" sphere like hexagonal bilayer as a precursor phase, before (100)/(100) interactions between NCs pull them together. Losing solvent molecules from the ligand shell before this precursor phase causes too much contraction, resulting in square-like superstructures.[22,27,40,48−50] We therefore hypothesize that the removal of the solvent early in the hexagonal (bi)layer precursor phase, changes the NC self-assembly from barely interactive NCs at long NC−NC distances to an assembly with attractive interactions resulting in a denser structure with shorter NC−NC distances. This indicates that the number of solvent molecules incorporated in the structure is critical for the stage at which (100)/(100) interactions come into play; if this occurs in an early stage, square-type monolayers are favored, while assembly under a nearly solvent-saturated atmosphere favors large bilayer domains that eventually evolve in buckled honeycomb structures.

SAED Analysis of NC Alignment during Honeycomb Formation. A way to study the NC alignment in this experiment is to analyze the 200 and 220 diffraction rings in SAED patterns. The total intensity of the rings, as compared to a powder diffraction pattern of bulk PbSe gives information on the percentage of NCs with a random orientation that are still present in the selected area. Table 1 lists the percentage of NCs in a random orientation observed in the experiments of Figure 3, which gradually decreases from 32 to 3% (see Supporting Information 5). At the same time, an interference pattern of six peaks begins to emerge on the 220 ring. In Figure 3c, this 220 ring is represented as an azimuthal trace (blue), and the six peaks are fitted with Gaussians (red). This provides quantitative values for the FWHM of the peaks during the entire 24 h after the dispersion was dropcasted on the liquid substrate. Additionally, the decreasing background intensity of the ring shows the increasing percentage of NCs aligned to neighboring NCs. To validate this analysis, the measured superlattice values are compared to the instrumentational broadening and background values, measured with a molybdenum single crystal.

Table 1. Overview of the Average Peak Width and the Percentage of Background Scattering[a]

time [h]	NCs with random orientation [%]	NCs aligned to neighboring NCs [%]	average 220 peak width [deg]
6	32	64	6.1
9	13	86	5.0
12	12	86	4.5
15	4	96	2.7
24	3	92	2.7

[a]The data is extracted from SAED patterns at different stages after NC deposition, for further discussion see Supporting Information 5.

Over the 6−15 h period, the 220 peak widths gradually decrease from 6.1 to 2.7°, while the overall percentage of oriented and aligned NCs increases from 64 to 96%, due to the increasing order in bilayers, i.e., a smaller and smaller number of PbSe NCs have a random rotation. However, for all of the SAED values, after 15 h, no further improvement of the alignment is observed, suggesting that irreversible necking between the (100)/(100) facets has occurred. The decreasing trend of randomly oriented NCs (Table 1, column 2) corresponds to the increasing percentage of NCs aligned to neighboring NCs (Table 1, column 3) and the decrease in average peak width (Table 1, column 4). This suggests that the alignment in the last stages of the process is caused by NC reorientations, which maximize the (100)/(100) attractions between NC neighbors. Other sources of NC alignment, for example, caused by NC−interface interactions are therefore less likely.

After 15 h, linear attachment observed in the hexagonal monolayer region suggests that NCs in the bilayer are also attached, but the conclusive proof is still missing. This is complicated by the fact that attachment occurs in ⟨100⟩ directions,[6] which have a 45° angle compared to the substrate plane. Therefore, shading from PbSe NCs prevents direct observation of bonds in this structure. By rotating the TEM samples over a 45° angle, the connections become visible and NC attachment can be confirmed. In Figure 4, the TEM samples taken at 9 and 15 h are shown at a 0° and 45° tilt. At a 45° rotation, the simple cubic bonding pattern[32,51] of the silicene-type honeycomb structure becomes clearly visible.

The sample taken at 9 h shows that all of the PbSe NCs are aligned and face each other via {100} facets, but except for a few positions, crystalline necks between nanocrystals are not present. This suggests that the NC alignment is driven by attractive interactions between these facets, resulting in an average peak width of 5.0° at the 220 ring. In contrast, the sample acquired after 15 h shows that nearly each NC in the structure has necks to its nearest neighbors (with a maximum of three in a silicene-type honeycomb structure). Therefore, this sample represents an attached honeycomb superlattice, with the smallest peak width of 2.7°.

The combination of all experiments shown above points to three distinct steps in the formation of honeycomb superlattices: (1) the formation of a well-ordered hexagonal bilayer, from unconnected "hard sphere like" NCs with the solvent incorporated in the ligand shell, as a "precursor" phase, (2) increasing alignment of NCs driven by (100)/(100) interactions, and (3) NC attachment by the formation of necks between nanocrystals, resulting in the final super-

https://doi.org/10.1021/acs.jpcc.1c07430
J. Phys. Chem. C 2022, 126, 986−996

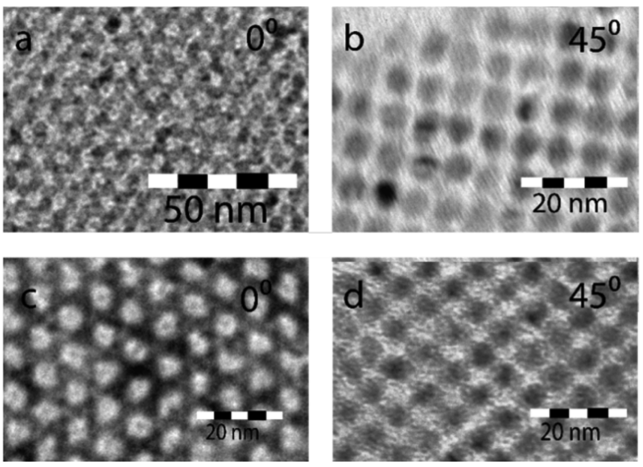

Figure 4. Electron tomography of a PbSe NC bilayer (a, b) and honeycomb superstructure (c, d) obtained after 9 and 15 h, respectively. (a) TEM image after 9 h viewed in the ⟨111⟩ direction, while panel (b) shows a TEM image of the same sample with a 45° tilted TEM grid. Similar for (c, d), except that the sample is taken after 15 h. Note that the top view of the nontilted samples (a, c) looks similar. When tilted, the images show the simple cubic structure in which NCs are not attached in (b), while crystalline necks have formed in (d).

structure. To achieve long-range order, separation of these steps is crucial; this means that the precursor phase should result in large well-ordered domains, which should be retained until NC alignment due to (100)/(100) attraction occurs.

Modelling Superstructure Formation for NCs with Different Repulsion Potentials. As indicated by earlier theoretical predictions,[52] NCs fully covered by ligands are thought to have rotational freedom at the solvent−air interface, while NCs having ligands chemisorbed only on their {110} and {111} facets, but not on their {100} facets, are expected to have a preferred orientation (with a (111) facet up) at the solvent−air interface. Therefore, it was previously thought that the interface-induced orientation of NCs could play a role in the formation of the buckled honeycomb structure.[52−54] In previous models, the self-assembly pathway was based on an early NC orientation at the solvent−air interface to move to the correct position to form square or honeycomb superlattices. However, the ex situ, real-time study of superlattice formation presented above shows the importance of a well-ordered hexagonal bilayer before the introduction of the (100)/(100) interaction for the alignment of NCs (see Figures 2e, 2f, and 3a).

To further investigate the self-assembly pathway, we present results from coarse-grained molecular dynamics simulations of up to 10^4 NCs. In these simulations, each NC is modeled as a polybead structure with a rhombicuboctahedron shape of roughly 6 nm (Supporting Information 6, Figure S11), where each bead in the structure represents a few atoms. Such a simplified coarse-grained model requires a lower computational cost for the simulations than a fully atomistic model, allowing the study of larger-scale systems. The dynamics of NCs are simulated using the position-Verlet algorithm,[55] while the distance between beads belonging to the same NC is kept fixed by constrained forces.[56] Bead−bead pair potentials are used to reproduce the NC−NC short-range facet-specific interactions, while the solvent is treated implicitly by modeling the NC Brownian motion. Further details on this model are reported in Supporting Information 6 and a recent publication.[53] In the simulations presented here, up to 10^4 NCs are initially randomly dispersed in a cubic box of side L aligned with a Cartesian coordinate system x,y,z and with periodic boundary conditions. The external force $-\mathrm{d}U_{2D}(z_c)/\mathrm{d}z_c$ is applied to each NC center of mass, with z_c the z coordinate of the NC center of mass, to model the effect of the evaporating solvent, which compresses the NCs in a 2D plane. The external potential U_{2D} is defined as

$$U_{2D}(z_c) = \begin{cases} u_z(z_c)^2, & \text{if } z_c < 0 \\ u_z(z_c - 4)^2, & \text{if } z_c > 4 \text{ nm} \end{cases}$$

Basically, NCs only feel an external force if their center of mass is not within a planar film of 4 nm thickness, then their center of mass is pushed toward this film forcing NCs to form a self-assembled mono- or bilayer. The parameter u_z is 10^{-19} J, in line with predicted solvent−air adsorption potentials of NCs.[53] During the first 0.1 μs of simulation, the beads of different NCs interact with each other only by a soft repulsive pair potential, mimicking the effect of ligand molecules chemisorbed on the NC surface

$$U_R(r) = \begin{cases} \in_R[(\sigma_R/r)^6] - 1, & \text{if } r \le \sigma_R \\ 0, & \text{otherwise} \end{cases}$$

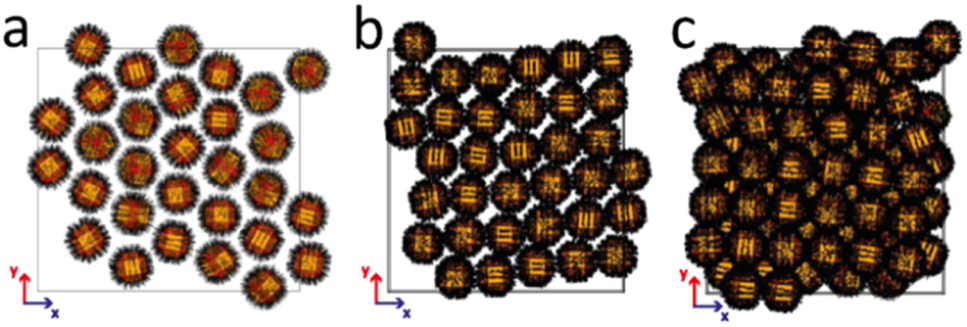

Figure 5. Top view of the quasi-2D structure formed in a molecular dynamics simulation with different parameters. In panels (a−c), NCs are randomly dispersed in a 3D box with dimensions L = 70 nm at the beginning and L = 32 nm at the end of the simulation, but before {100} facet attraction is turned on. In panel (a) with a $\epsilon_R = 8 \times 10^{-21}$ J repulsion, a free rotational hexagonal structure is formed. In panels (b, c) with a $\epsilon_R = 0.2 \times 10^{-21}$ J repulsion, a square structure with predominantly {100} facets up is formed both in the monolayer (with 35 NCs) and double layer (with 70 NCs) simulation.

https://doi.org/10.1021/acs.jpcc.1c07430
J. Phys. Chem. C 2022, 126, 986−996

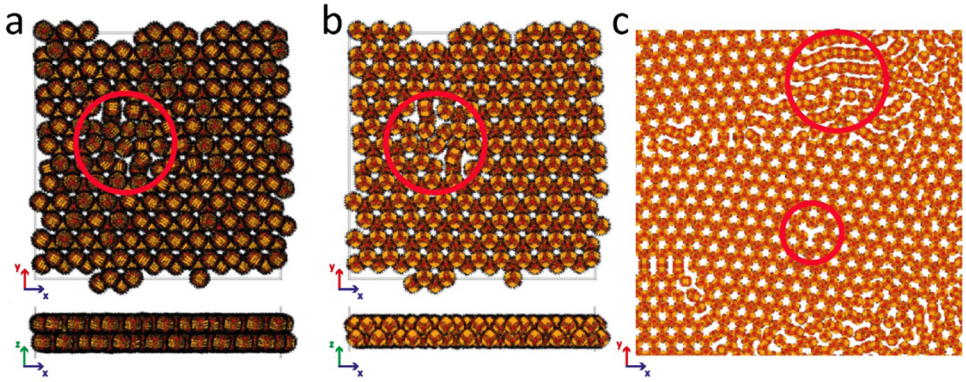

Figure 6. Top view of the quasi-2D structure formed in large-scale molecular dynamic simulations. In panels (a,b), the top and side views of a simulation with 280 NCs are shown with only repulsive potential (a) and with {100} facet−facet attraction turned on (b). In panel (a), a hexagonal double layer is formed with areas of (100) facet up (yellow facet) and (111) facet up (red). This hexagonal double layer then evolves to a silicene-type honeycomb superstructure (b). In panel (c), a zoomed-in portion of Figure S12 is shown, a simulation with 10^4 randomly dispersed NCs in a 3D box of sides L = 620 nm compressed in a thin planar film. NC−NC attraction by {100} facets (yellow) is switched on after 0.1 μs forming domains of silicene-type honeycomb superstructures. The red circles indicate defect areas in all simulations, which are shown in detail in Figure S13.

where r is the bead−bead center-of-mass distance, ϵ_R is the magnitude of the repulsive potential, and σ_R is the ligand length. After 0.1 μs, the attractive pair potentials between beads belonging to NCs' {100} facets are (gradually) turned on, mimicking ligands detaching from {100} facets (thus allowing the facet−facet interaction). This second simulation phase, in which NCs attract each other by {100} facets, is continued for at least 0.05 μs. A complete overview of the parameters used in the simulations is reported in Supporting Information 6.

Initially, we performed small-scale simulations, with 35 and 70 NCs, for only the first phase, i.e., before turning on attractions between {100} facets. The NCs are placed in a box shrinking linearly from L = 70 nm (at the beginning) to L = 32 nm (at the end of the simulation), to simulate the evaporating solvent. This reduction is slow enough to allow equilibration of NCs. The resulting top view (the z-direction is orthogonal to the paper plane) of these simulations is shown in Figure 5.

When NCs are allowed to self-assemble with a strong repulsive potential (of $\epsilon_R = 8 \times 10^{-21}$ J, Figure 5a), emulating NCs with a full ligand shell and solvent inclusion, a hexagonal monolayer is formed by randomly oriented NCs. However, in simulations with a lower repulsive potential (of $\epsilon_R = 0.2 \times 10^{-21}$ J), the particle shape becomes more dominant during the self-assembly. Then, square geometries are formed with the particles predominantly oriented with their {100} facets up, both in the monolayer and the bilayer (Figure 5b, 5c). It is an indication that with high repulsive potential, both in simulation and under experimental conditions with high solvent vapor pressure (Figures 1a and 2e, 2f), the particles can self-assemble like barely interactive (hard) spheres and form hexagonal geometries with free orientation.

In larger simulations with 280 NCs, the entire attachment process was studied in two phases. During the first simulation phase (Figure 6a), the soft repulsive pair potential again emulates a full ligand corona with solvent inclusion, allowing NCs to self-assemble as barely interacting spheres. Then, during the second phase, the facet−facet interaction is gradually turned on (Figure 6b). Both the top view and side view are displayed at the end of each simulation phase. As NCs only interact via a soft repulsive pair potential during the first phase, they self-assemble into a hexagonal double layer, with some particle orientation of (100) and (111) facet up. During the second simulation phase, the overall thickness of the double layer decreases, as the facet−facet interaction allows a closer approach of NCs. At the same time, the previously formed hexagonal bilayer clearly evolves into a silicene-type honeycomb structure. The honeycomb structure is formed both in the areas initially showing PbSe NCs with ⟨111⟩ orientation and ⟨100⟩ orientation. An indication that the formation of the ordered precursor phase, a double hexagonal layer without aligned NCs, is more important than the individual NC orientation in the initial stages of the self-assembly. The increasing alignment of nanocrystals agrees with our experimental observations (Table 1). In addition, the defects observed in the self-assembly phase and after attachment are very similar (red circles in Figure 6) to what we already observed. These defects are discussed further in Figure S13.

In simulations performed at an even larger scale with 10^4 NCs, the final structure is obtained with L = 620 nm and the complete simulation is shown in Figure S12 (Figure 6c shows a part of Figure S12). The formation of silicene-type honeycomb superstructures, by turning on attractions between NC {100} facets, is observed only in areas where a hexagonal bilayer precursor phase was preformed.

The results obtained in simulations suggest that a coarse-grained model can reproduce the NC self-assembly and the defects in the structure. The results corroborate the hypothesis that for honeycomb formation, a large steric repulsion is needed during the self-assembly of NCs to form hexagonal double layers. In experiments, this was achieved using nearly solvent-saturated conditions, which swell the ligand corona.[27,28,48,50,57] Previous works on the self-assembly of NCs show that this causes a larger NC−NC separation and more repulsion.[27,28,48,57−59] The results of time-monitoring reported here, supported by large-scale simulations with compressive and slow solvent evaporation, show that honeycomb formation is driven by the formation of hexagonal bilayers in a confined quasi-2D space. NCs not (yet) aligned with the ⟨111⟩ axis upwards, in the hexagonal bilayer, are able to reorient, allowing for maximal attraction between opposing (100) facets and eventually neck formation.

https://doi.org/10.1021/acs.jpcc.1c07430
J. Phys. Chem. C 2022, 126, 986−996

CONCLUSIONS

We show that the formation of PbSe honeycomb superstructures proceeds via the following sequence: NC self-assembly, alignment, and oriented attachment. Both the experimental and model results show that to achieve high-quality long-range superstructures, it is important that these steps are separated. Therefore, it is crucial that (100)/(100) attractive interactions do not dominate during the self-assembly phase. If facet attractions occur in a too early stage, small domains with square and linear attachments break long-range order in an irreversible way. Experimentally, long-range self-assembly was achieved by the addition of less reactive 1,4-butanediol to the reactive ethylene glycol liquid substrate, which helps to control the facet reactivity. In addition to the quality, the type of two-dimensional superstructure will be determined by the self-assembly process. At a high solvent vapor pressure, the relatively open hexagonal double layer will be stabilized during the self-assembly, as solvent molecules included in the NC ligand shell allow NCs to act more like "hard spheres." When ligands are removed during this organization, NCs will align under the influence of attractive (100)/(100) attractions and finally attach irreversibly to form a honeycomb superstructure.

ASSOCIATED CONTENT

Supporting Information

The Supporting Information is available free of charge at https://pubs.acs.org/doi/10.1021/acs.jpcc.1c07430.

The supporting information contains additional TEM images of superlattice formation on different liquid substrates, a short discussion of a potential mechanism for ligand stripping, a table with chemical properties of the liquid substrates, NMR and FTIR data showing the ligand density determination, a discussion of lower magnification TEM images of hexagonal bilayers and honeycomb superstructures, calculations of different volumes in an NC, further discussion of the SAED analysis in Table 1, further details on the parameters used in the simulations, an additional large-scale simulation result, and a discussion of the defects observed both in experiments and simulations (PDF)

AUTHOR INFORMATION

Corresponding Author

Joep L. Peters − *Condensed Matter and Interfaces, Debye Institute for Nanomaterials Science, University of Utrecht, 3584 CC Utrecht, The Netherlands;* orcid.org/0000-0002-3415-648X; Email: joeppeters89@gmail

Authors

Maaike M. van der Sluijs − *Condensed Matter and Interfaces, Debye Institute for Nanomaterials Science, University of Utrecht, 3584 CC Utrecht, The Netherlands;* orcid.org/0000-0001-7097-5506

Dinja Sanders − *Condensed Matter and Interfaces, Debye Institute for Nanomaterials Science, University of Utrecht, 3584 CC Utrecht, The Netherlands*

Kevin J. Jansen − *Condensed Matter and Interfaces, Debye Institute for Nanomaterials Science, University of Utrecht, 3584 CC Utrecht, The Netherlands*

Giuseppe Soligno − *Condensed Matter and Interfaces, Debye Institute for Nanomaterials Science, University of Utrecht, 3584 CC Utrecht, The Netherlands;* Present Address: Soligno Technologies, Utrecht, The Netherlands; orcid.org/0000-0003-2360-2082

Daniel Vanmaekelbergh − *Condensed Matter and Interfaces, Debye Institute for Nanomaterials Science, University of Utrecht, 3584 CC Utrecht, The Netherlands;* orcid.org/0000-0002-3535-8366

Complete contact information is available at: https://pubs.acs.org/10.1021/acs.jpcc.1c07430

Author Contributions

The manuscript was written through the contributions of all authors. All authors have given approval to the final version of the manuscript.

Notes

The authors declare no competing financial interest.

ACKNOWLEDGMENTS

D.V., G.S., and M.M.v.d.S. acknowledge the ERC Advanced Grant "First Step" No. 692691. J.P. acknowledges the Dutch FOM program "Designing Dirac carriers in honeycomb semiconductor superlattices" (FOM Program 152) for financial support. D.V. acknowledges The Netherlands Organization for Scientific Research (NWO) TOP-grant with Project No. 715.016.002.

ABBREVIATIONS USED

2D, two-dimensional; 3D, three-dimensional; BD, 1,4-butanediol; DEG, diethylene glycol; EG, ethylene glycol; GISAXS/GIWAXS, grazing-incidence small- and wide-angle X-ray scattering; NCs, nanocrystals; TEM, transmission electron microscopy; SAED, selected-area electron diffraction

REFERENCES

(1) Franchina Vergel, N. A.; Post, L. C.; Sciacca, D.; Berthe, M.; Vaurette, F.; Lambert, Y.; Yarekha, D.; Troadec, D.; Coinon, C.; Fleury, G.; et al. Engineering a Robust Flat Band in III−V Semiconductor Heterostructures. *Nano Lett.* **2021**, *21*, 680−685.

(2) Post, L. C.; Xu, T.; Franchina Vergel, N. A.; Tadjine, A.; Lambert, Y.; Vaurette, F.; Yarekha, D.; Desplanque, L.; Stievenard, D.; Wallart, X.; et al. Triangular Nanoperforation and Band Engineering of InGaAs Quantum Wells: A Lithographic Route toward Dirac Cones in III-V Semiconductors. *Nanotechnology* **2019**, *30*, No. 155301.

(3) Evers, W. H.; Goris, B.; Bals, S.; Casavola, M.; de Graaf, J.; van Roij, R.; Dijkstra, M.; Vanmaekelbergh, D. Low-Dimensional Semiconductor Superlattices Formed by Geometric Control over Nanocrystal Attachment. *Nano Lett.* **2013**, *13*, 2317−2323.

(4) Yao, K. X.; Yin, X. M.; Wang, T. H.; Zeng, H. C. Synthesis, Self-Assembly, Disassembly, and Reassembly of Two Types of Cu2O Nanocrystals Unifaceted with {001} or {110} Planes. *J. Am. Chem. Soc.* **2010**, *132*, 6131−6144.

(5) Baumgardner, W. J.; Whitham, K.; Hanrath, T. Confined-but-Connected Quantum Solids Via Controlled Ligand Displacement. *Nano Lett.* **2013**, *13*, 3225−3231.

(6) Boneschanscher, M. P.; Evers, W. H.; Geuchies, J. J.; Altantzis, T.; Goris, B.; Rabouw, F. T.; van Rossum, S. A.; van der Zant, H. S.; Siebbeles, L. D.; Van Tendeloo, G.; et al. Long-Range Orientation and Atomic Attachment of Nanocrystals in 2D Honeycomb Superlattices. *Science* **2014**, *344*, 1377−1380.

(7) Nakagawa, Y.; Kageyama, H.; Oaki, Y.; Imai, H. Formation of Monocrystalline 1D and 2D Architectures Via Epitaxial Attachment: Bottom-up Routes through Surfactant-Mediated Arrays of Oriented Nanocrystals. *Langmuir* **2015**, *31*, 6197−6201.

(8) Salzmann, B. B. V.; van der Sluijs, M. M.; Soligno, G.; Vanmaekelbergh, D. Oriented Attachment: From Natural Crystal Growth to a Materials Engineering Tool. *Acc. Chem. Res.* **2021**, *54*, 787−797.
(9) Peters, J. L.; van den Bos, K. H. W.; Van Aert, S.; Goris, B.; Bals, S.; Vanmaekelbergh, D. Ligand-Induced Shape Transformation of PbSe Nanocrystals. *Chem. Mater.* **2017**, *29*, 4122−4128.
(10) Hanrath, T. Colloidal Nanocrystal Quantum Dot Assemblies as Artificial Solids. *J. Vac. Sci. Technol. A* **2012**, *30*, No. 030802.
(11) Delerue, C. From Semiconductor Nanocrystals to Artificial Solids with Dimensionality Below Two. *Phys. Chem. Chem. Phys.* **2014**, *16*, 25734−25740.
(12) Kalesaki, E.; Evers, W. H.; Allan, G.; Vanmaekelbergh, D.; Delerue, C. Electronic Structure of Atomically Coherent Square Semiconductor Superlattices with Dimensionality Below Two. *Phys. Rev. B* **2013**, *88*, No. 115431.
(13) Kalesaki, E.; Delerue, C.; Morais Smith, C.; Beugeling, W.; Allan, G.; Vanmaekelbergh, D. Dirac Cones, Topological Edge States, and Nontrivial Flat Bands in Two-Dimensional Semiconductors with a Honeycomb Nanogeometry. *Phys. Rev. X* **2014**, *4*, No. 011010.
(14) Delerue, C.; Vanmaekelbergh, D. Electronic Band Structure of Zinc Blende CdSe and Rock Salt PbSe Semiconductors with Silicene-Type Honeycomb Geometry. *2D Mater.* **2015**, *2*, No. 034008.
(15) Yang, H. G.; Zeng, H. C. Self-Construction of Hollow SnO(2) Octahedra Based on Two-Dimensional Aggregation of Nanocrystallites. *Angew. Chem. Int. Ed.* **2004**, *43*, 5930−5933.
(16) Liu, B.; Zeng, H. C. Mesoscale Organization of CuO Nanoribbons: Formation of ″Dandelions″. *J. Am. Chem. Soc.* **2004**, *126*, 8124−8125.
(17) Cölfen, H.; Antonietti, M. Mesocrystals: Inorganic Superstructures Made by Highly Parallel Crystallization and Controlled Alignment. *Angew. Chem. Int. Ed.* **2005**, *44*, 5576−5591.
(18) Imai, H. Mesostructured Crystals: Growth Processes and Features. *Prog. Cryst. Growth Charact. Mater.* **2016**, *62*, 212−226.
(19) Geuchies, J. J.; van Overbeek, C.; Evers, W. H.; Goris, B.; de Backer, A.; Gantapara, A. P.; Rabouw, F. T.; Hilhorst, J.; Peters, J. L.; Konovalov, O.; et al. In Situ Study of the Formation Mechanism of Two-Dimensional Superlattices from PbSe Nanocrystals. *Nat. Mater.* **2016**, *15*, 1248−1254.
(20) Radha, B.; Senesi, A. J.; O'Brien, M. N.; Wang, M. X.; Auyeung, E.; Lee, B.; Mirkin, C. A. Reconstitutable Nanoparticle Superlattices. *Nano Lett.* **2014**, *14*, 2162−2167.
(21) Wei, J.; Schaeffer, N.; Pileni, M.-P. Solvent-Mediated Crystallization of Nanocrystal 3D Assemblies of Silver Nanocrystals: Unexpected Superlattice Ripening. *Chem. Mater.* **2016**, *28*, 293−302.
(22) Fan, Z.; Grunwald, M. Orientational Order in Self-Assembled Nanocrystal Superlattices. *J. Am. Chem. Soc.* **2019**, *141*, 1980−1988.
(23) Winslow, S. W.; Swan, J. W.; Tisdale, W. A. The Importance of Unbound Ligand in Nanocrystal Superlattice Formation. *J. Am. Chem. Soc.* **2020**, *142*, 9675−9685.
(24) Li, D.; Nielsen, M. H.; Lee, J. R.; Frandsen, C.; Banfield, J. F.; De Yoreo, J. J. Direction-Specific Interactions Control Crystal Growth by Oriented Attachment. *Science* **2012**, *336*, 1014−1018.
(25) Walravens, W.; De Roo, J.; Drijvers, E.; Ten Brinck, S.; Solano, E.; Dendooven, J.; Detavernier, C.; Infante, I.; Hens, Z. Chemically Triggered Formation of Two-Dimensional Epitaxial Quantum Dot Superlattices. *ACS Nano* **2016**, *10*, 6861−6870.
(26) van Overbeek, C.; Peters, J. L.; van Rossum, S. A. P.; Smits, M.; van Huis, M. A.; Vanmaekelbergh, D. Interfacial Self-Assembly and Oriented Attachment in the Family of PbX (X = S, Se, Te) Nanocrystals. *J. Phys. Chem. C* **2018**, *122*, 12464−12473.
(27) Bian, K.; Choi, J. J.; Kaushik, A.; Clancy, P.; Smilgies, D. M.; Hanrath, T. Shape-Anisotropy Driven Symmetry Transformations in Nanocrystal Superlattice Polymorphs. *ACS Nano* **2011**, *5*, 2815−2823.
(28) Missoni, L. L.; Tagliazucchi, M. The Phase Behavior of Nanoparticle Superlattices in the Presence of a Solvent. *ACS Nano* **2020**, *14*, 5649−5658.
(29) Steckel, J. S.; Coe-Sullivan, S.; Bulović, V.; Bawendi, M. G. 1.3μm to 1.55μm Tunable Electroluminescence from PbSe Quantum Dots Embedded within an Organic Device. *Adv. Mater.* **2003**, *15*, 1862−1866.
(30) Campos, M. P.; Hendricks, M. P.; Beecher, A. N.; Walravens, W.; Swain, R. A.; Cleveland, G. T.; Hens, Z.; Sfeir, M. Y.; Owen, J. S. A Library of Selenourea Precursors to PbSe Nanocrystals with Size Distributions near the Homogeneous Limit. *J. Am. Chem. Soc.* **2017**, *139*, 2296−2305.
(31) Hendricks, M. P.; Campos, M. P.; Cleveland, G. T.; Jen-La Plante, I.; Owen, J. S. A Tunable Library of Substituted Thiourea Precursors to Metal Sulfide Nanocrystals. *Science* **2015**, *348*, 1226−1230.
(32) Peters, J. L.; Altantzis, T.; Lobato, I.; Jazi, M. A.; van Overbeek, C.; Bals, S.; Vanmaekelbergh, D.; Sinai, S. B. Mono- and Multilayer Silicene-Type Honeycomb Lattices by Oriented Attachment of PbSe Nanocrystals: Synthesis, Structural Characterization, and Analysis of the Disorder. *Chem. Mater.* **2018**, *30*, 4831−4837.
(33) Moreels, I.; Lambert, K.; De Muynck, D.; Vanhaecke, F.; Poelman, D.; Martins, J. C.; Allan, G.; Hens, Z. Composition and Size-Dependent Extinction Coefficient of Colloidal PbSe Quantum Dots. *Chem. Mater.* **2007**, *19*, 6101−6106.
(34) Geuchies, J. J.; Soligno, G.; Geraffy, E.; Hendrikx, C. P.; van Overbeek, C.; Montanarella, F.; Slot, M. R.; Konovalov, O. V.; Petukhov, A. V.; Vanmaekelbergh, D., Unravelling Three-Dimensional Adsorption Geometries of PbSe Nanocrystal Monolayers at a Liquid-Air Interface. *Commun. Chem.* **2020** *3*, DOI: 10.1038/s42004-020-0275-4.
(35) Hassinen, A.; Moreels, I.; De Nolf, K.; Smet, P. F.; Martins, J. C.; Hens, Z. Short-Chain Alcohols Strip X-Type Ligands and Quench the Luminescence of PbSe and CdSe Quantum Dots, Acetonitrile Does Not. *J. Am. Chem. Soc.* **2012**, *134*, 20705−20712.
(36) Owen, J. S. The Coordination Chemistry of Nanocrystal Surfaces. *Science* **2015**, *347*, 615−616.
(37) Fritzinger, B.; Capek, R. K.; Lambert, K.; Martins, J. C.; Hens, Z. Utilizing Self-Exchange to Address the Binding of Carboxylic Acid Ligands to CdSe Quantum Dots. *J. Am. Chem. Soc.* **2010**, *132*, 10195−10201.
(38) Abelson, A.; Qian, C.; Salk, T.; Luan, Z.; Fu, K.; Zheng, J. G.; Wardini, J. L.; Law, M. Collective Topo-Epitaxy in the Self-Assembly of a 3D Quantum Dot Superlattice. *Nat. Mater.* **2020**, *19*, 49−55.
(39) Anderson, N. C.; Hendricks, M. P.; Choi, J. J.; Owen, J. S. Ligand Exchange and the Stoichiometry of Metal Chalcogenide Nanocrystals: Spectroscopic Observation of Facile Metal-Carboxylate Displacement and Binding. *J. Am. Chem. Soc.* **2013**, *135*, 18536−18548.
(40) Weidman, M. C.; Smilgies, D. M.; Tisdale, W. A. Kinetics of the Self-Assembly of Nanocrystal Superlattices Measured by Real-Time in Situ X-Ray Scattering. *Nat. Mater.* **2016**, *15*, 775−781.
(41) Bain, E. C.; Dunkirk, N. The Nature of Martensite. *Trans. AIME* **1924**, *70*, 25−47.
(42) Lee, B.; Littrell, K.; Sha, Y.; Shevchenko, E. V. Revealing the Effects of the Non-Solvent on the Ligand Shell of Nanoparticles and Their Crystallization. *J. Am. Chem. Soc.* **2019**, *141*, 16651−16662.
(43) Maiti, S.; Andre, A.; Maiti, S.; Hodas, M.; Jankowski, M.; Scheele, M.; Schreiber, F. Revealing Structure and Crystallographic Orientation of Soft Epitaxial Assembly of Nanocrystals by Grazing Incidence X-Ray Scattering. *J. Phys. Chem. Lett.* **2019**, *10*, 6324−6330.
(44) Quan, Z.; Wu, D.; Zhu, J.; Evers, W. H.; Boncella, J. M.; Siebbeles, L. D.; Wang, Z.; Navrotsky, A.; Xu, H. Energy Landscape of Self-Assembled Superlattices of PbSe Nanocrystals. *Proc. Natl. Acad. Sci. U.S.A.* **2014**, *111*, 9054−9057.
(45) Wang, Z.; Schliehe, C.; Bian, K.; Dale, D.; Bassett, W. A.; Hanrath, T.; Klinke, C.; Weller, H. Correlating Superlattice Polymorphs to Internanoparticle Distance, Packing Density, and Surface Lattice in Assemblies of PbS Nanoparticles. *Nano Lett.* **2013**, *13*, 1303−1311.
(46) Zaluzhnyy, I. A.; Kurta, R. P.; Andre, A.; Gorobtsov, O. Y.; Rose, M.; Skopintsev, P.; Besedin, I.; Zozulya, A. V.; Sprung, M.;

Schreiber, F.; et al. Quantifying Angular Correlations between the Atomic Lattice and the Superlattice of Nanocrystals Assembled with Directional Linking. *Nano Lett.* **2017**, *17*, 3511−3517.
(47) Choi, J. J.; Bealing, C. R.; Bian, K.; Hughes, K. J.; Zhang, W.; Smilgies, D. M.; Hennig, R. G.; Engstrom, J. R.; Hanrath, T. Controlling Nanocrystal Superlattice Symmetry and Shape-Anisotropic Interactions through Variable Ligand Surface Coverage. *J. Am. Chem. Soc.* **2011**, *133*, 3131−3138.
(48) Wan, Y.; Goubet, N.; Albouy, P. A.; Schaeffer, N.; Pileni, M. P. Hierarchy in Au Nanocrystal Ordering in a Supracrystal: II. Control of Interparticle Distances. *Langmuir* **2013**, *29*, 13576−13581.
(49) Quan, Z.; Xu, H.; Wang, C.; Wen, X.; Wang, Y.; Zhu, J.; Li, R.; Sheehan, C. J.; Wang, Z.; Smilgies, D. M.; et al. Solvent-Mediated Self-Assembly of Nanocube Superlattices. *J. Am. Chem. Soc.* **2014**, *136*, 1352−1359.
(50) Kaushik, A. P.; Clancy, P. Solvent-Driven Symmetry of Self-Assembled Nanocrystal Superlattices–a Computational Study. *J. Comput. Chem.* **2013**, *34*, 523−532.
(51) Tadjine, A.; Delerue, C. Colloidal Nanocrystals as Lego(R) Bricks for Building Electronic Band Structure Models. *Phys. Chem. Chem. Phys.* **2018**, *20*, 8177−8184.
(52) Soligno, G.; Vanmaekelbergh, D. Phase Diagrams of Honeycomb and Square Nanocrystal Superlattices from the Nanocrystal's Surface Chemistry at the Dispersion-Air Interface. *J. Chem. Phys.* **2019**, *151*, No. 234702.
(53) Soligno, G.; Vanmaekelbergh, D. Understanding the Formation of PbS Honeycomb Superstructures by Dynamics Simulations. *Phys. Rev. X* **2019**, *9*, No. 021015.
(54) Gupta, U.; Escobedo, F. A. Implicit Solvent Model for the Interfacial Configuration of Colloidal Nanoparticles and Application to the Self-Assembly of Truncated Cubes. *J. Chem. Theory Comput.* **2020**, *16*, 5866−5875.
(55) Frenkel, D.; Smit, B. *Understanding Molecular Simulation: From Algorithms to Applications*; Elsevier, 2002.
(56) Ciccotti, G.; Ryckaert, J. P. Molecular-Dynamics Simulation of Rigid Molecules. *Comput. Phys. Rep.* **1986**, *4*, 346−392.
(57) Zhang, J.; Luo, Z.; Martens, B.; Quan, Z.; Kumbhar, A.; Porter, N.; Wang, Y.; Smilgies, D. M.; Fang, J. Reversible Kirkwood-Alder Transition Observed in Pt3Cu2 Nanoctahedron Assemblies under Controlled Solvent Annealing/Drying Conditions. *J. Am. Chem. Soc.* **2012**, *134*, 14043−14049.
(58) Pool, R.; Schapotschnikow, P.; Vlugt, T. J. H. Solvent Effects in the Adsorption of Alkyl Thiols on Gold Structures: A Molecular Simulation Study. *J. Phys. Chem. C* **2007**, *111*, 10201−10212.
(59) Goubet, N.; Richardi, J.; Albouy, P.-A.; Pileni, M.-P. Which Forces Control Supracrystal Nucleation in Organic Media? *Adv. Funct. Mater.* **2011**, *21*, 2693−2704.

https://doi.org/10.1021/acs.jpcc.1c07430
J. Phys. Chem. C 2022, 126, 986−996